THE EFFECT OF COOLING RATE ON THE MICROSTRUCTURE AND HARDNESS OF AS-CAST Co-28Cr-6Mo ALLOY USED AS BIOMEDICAL KNEE IMPLANT

Douglas Júnior da Silva, Rodrigo Contieri, Alessandra Cremasco and Ricardo Floriano
Laboratory of Materials (LabMat), School of Applied Sciences, University of Campinas (FCA-UNICAMP), Pedro Zaccaria, 1300, Limeira 13484-350, Brazil

https://doi.org/10.1007/s40962-021-00749-7

Abstract

Co-based alloys are currently the most suitable material used for hip and knee joint replacements due to their good biocompatibility, high strength, wear resistance and high corrosion resistance. In this study, the effects of cooling rate on the microstructure and hardness in different regions of a commercial knee implant (tibial implant) of the as-cast Co-28Cr-6Mo alloy (ASTM F75) processed under industrial conditions were evaluated. The X-ray diffraction (XRD) patterns showed that the microstructure of as-cast Co-28Cr-6Mo alloy consists of two main phases: γ (FCC) and ε (HCP) phases. Scanning electron microscopy (SEM) together with Energy dispersive spectroscopy (EDS) analysis also revealed the presence of carbides with composition of (Cr, Co)C_6 which was found precipitated in the grain boundaries and in interdendritic regions. Porosity and a small fraction of oxides localized in regions of high free energy such as grain boundaries and carbides were also observed. Casting numerical simulation applied to the implant showed that the regions of implant with turbulent flow of the liquid metal were more susceptible to the presence of porosity and oxides. However, larger and more concentrated defects can lead to brittle failure of the tibial implant. The regions of the implant with high cooling rates presented grain refinement and, consequently, high hardness values. An increase in cooling rates from 2.2 to 30 °C/s promotes an increase of 48.5% in hardness. Besides, the rise in cooling rate did not affect the fraction of carbides, but promoted the formation of more refined carbides.

Received: 08 September 2021 / Accepted: 17 December 2021 /
Published online: 25 January 2022

Graphical Abstract

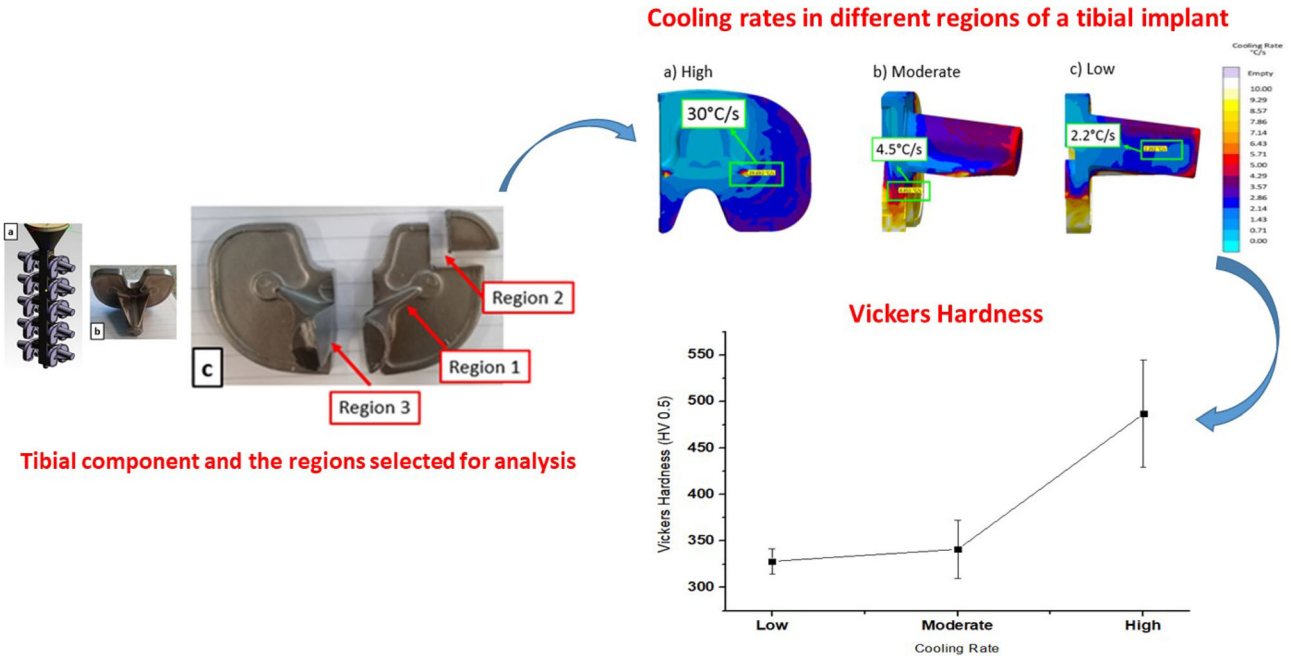

Keywords: *Co-Cr-Mo alloy, cooling rate, microstructure, knee implant, hardness property*

Introduction

Co-28Cr-6Mo alloys are commonly used for orthopedic implants such as knee and hip joint replacements due to their good biocompatibility and corrosion resistance, high strength, wear resistance and fatigue strength. [1]Furthermore, Co-based alloys possess higher fatigue strength and wear resistance in comparison to stainless steels and titanium alloys. [2]The knee implant is composed of tibial and femoral components, which are commonly produced by investment casting. This processing route is often the preferred method of manufacture of implants especially due to the complexity of the shape or design of implants as well as the poor machinability of the alloy. [3,4]Additive manufacturing (AM) routes such as selective laser melting (SLM) or electron beam melting (EBM) are promising technologies for producing biomedical devices as well as new alternative processing routes for replacing the investment casting. However, the main drawback of AM processes is the high amount of residual stresses due to the rapid cooling rate during the solidification, the high costs and limited productivity. [1]Besides, heat treatments such as solution annealing and hot isostatic pressing (HIP) are required on the as-printed alloy produced by AM to enhance the mechanical and corrosion behavior desired in implants. [2]Therefore, investment casting is still the preferred processing route for Co-based alloys used as biomedical materials even considering the need to apply thermo-mechanical treatments to homogenize the microstructure to reach the properties required for Co-based alloys (ASTM F75).

The typical microstructure of as-cast Co-28Cr-6Mo alloy (ASTM F75) has two main phases as namely: γ-phase (face-centered cubic (FCC) structure) and ε- phase (hexagonal close-packed (HCP) structure), which are thermodynamically stable at high and low temperatures, respectively. [1]The alloying elements play an important role on the microstructure of this alloy. On one hand, the additions of Fe, Ni, Mn and C elements stabilize the γ-phase at room temperature by lowering the γ-phase -> ε-phase transformation temperature under cooling. On the other hand, the additions of Cr, Mo, W and Si elements are ε-phase stabilizers because these elements increase the γ-phase -> ε-phase transformation temperature. [5]Besides the γ and ε- phases (Co-rich phases) found in the as-cast sate of alloy, the presence of carbides with constitution of around $M_{23}C_6$ is also found precipitated in the interdendritic zones and grain boundaries in the alloy. [6]Very fine carbides present at intra-granular regions and uniformly distributed in the matrix is one of the hardening mechanisms for this alloy, as well as solid solution strengthening[6] and dislocations interactions with stacking

fault intersections. [7]However, brittle carbides formed along to the grain boundaries is also responsible for the reduction of ductility and fatigue strength. Besides, the presence of carbides is also detrimental to the corrosion performance of Co-based alloys. [6]Other secondary phases including σ-phase and lamellar carbides were also reported in Co-Cr-Mo alloys. [8]Lamellar carbides are composed of interlayer plates of $Cr_{23}C_6$ and Co-γ dendritic matrix and are mainly found precipitated in the grain boundaries. [9]The amount of lamellar and blocky carbides was found to increase with carbon content[7].

It is well known that a posterior heat treatment applied to the as-cast alloy is an alternative method to enhance not only ductility but also other mechanical properties such as yield and ultimate tensile strengths. [10–12]Furthermore, heat treatments commonly used in these alloys also improve wear and prevent fatigue failure associated with the low ductility of the as-cast alloy. Normally, the procedure consists of a solution treatment carried out at temperatures between 1165 and 1270 °C for periods ranging from 1 to 4 h. The adequate choice of values for different heat treatments can induce total or partial dissolution of carbides of alloy affecting its mechanical and corrosion properties[11,12].

In particular, for the Co-28Cr-6Mo alloy used as Knee implant is crucial to understand the effects of the casting parameters on the microstructure of alloy to avoid any premature mechanical failure that might be caused by metallurgical defects as well as the presence of second phases of brittle nature. Among these casting parameters, the cooling rate is one of the most important parameter during the solidification of the molten metal. Kaiser et al.[3] investigated the effect of the cooling rate on the microstructure, secondary phase precipitates and mechanical properties of an as-cast Co-28Cr-6Mo alloy. It was shown that the cooling rate affects the secondary dendrite arm spacing (SDAS) of the Co-based alloys. The higher the cooling rate, the greater is the dendrite refinement. It was also reported that the rise in cooling rate enhances the tensile strength, hardness and yield strength, but, lowers ductility of the Co-Cr-Mo alloy. In another study performed by RAMÍREZ-VIDAURRI et al.[9], the effect of C content (0.45, 0.33, 0.36 and 0.25 wt%) and the cooling rate on the fraction of carbides in the Co-28Cr-6Mo alloy was evaluated. They reported that the cooling rate does not affect significantly the fraction of carbides present in the as-cast microstructures. However, it was found that the size of the carbides decreases as the cooling rate increases.

Most of the previous studies found in the literature[3, 5–12] whose focus is on the evaluation of the microstructure aspects related to the casting parameters in biomedical materials, in particular for Co-based alloys, are carried out using laboratorial scale casting parameters, and the microstructural analysis is normally performed using cylinders or tension test bars. In other words, the analysis of the microstructure is performed in a component out of the design of the real implant. Therefore, the local variations of the microstructure along with the real volume of an implant considering the complex geometry and its differences of thickness are no longer reported in the literature. Regarding to the implant fractures occurred in total knee replacement (TKR), clinical studies have shown a failure rate of the tibial implant of 285 per 100,000 patients. [13]These failures are rare in primary knee implants, but must be avoided to guarantee the patient's reliability regarding to the metallic biomaterial implantation. Mechanical failures might be related to the microstructural features of the alloy such as metallurgical defects as well as the presence of second phases of brittle nature. Considering the fact that the total knee arthroplasty (TKA) will increase in the US 284% until 2030 compared to 2014, according to the projections of Singh et al.[14], the understanding of the reasons of implant failures relies on a deep knowledge of its microstructure features.

In this study, we evaluated the microstructural differences of the as-cast Co-28Cr-6Mo (ASTM F75) alloy in three different regions of a commercial tibial implant obtained by investment casting under industrial conditions. The greatest contribution of this paper was to investigate the microstructural features directly in the commercial product to assess whether there are metallurgical defects and also second phases with brittle nature in different regions of implant. So, this investigation is of paramount importance once most of the mechanical failures reported by the literature[14,15] for tibial components occurred in one of the regions investigated (taken from the tibia baseplate) in this study. As already mentioned, most of the previous studies found in the literature[3,5–12] were carried out using laboratorial scale casting parameters, and the microstructural analysis was performed using samples with different geometry in comparison with the final product. However, it is well known that the geometry of the cast interferes on the solidification behavior of the alloy, and this study will provide more information on how the microstructure features change along the knee implant. Finally, casting numerical simulation was employed to evaluate the metal flow during mold filling and also to determine the cooling rates and temperature gradients within the solidification range in the regions investigated. As a result, it was possible to assess the effect of cooling rate on the microstructure and hardness of the alloy.

Materials and Methods

The as-cast tibial component with a nominal composition of Co-28Cr-6Mo according to the ASTM F75 was produced by investment casting under industrial conditions. An induction furnace with a capacity of 150 kg was used to melt the alloy. During the melting, furnace atmosphere control was not employed, however, metallic silicon with 99.10% of purity and with sizes around 3–5 mm was added

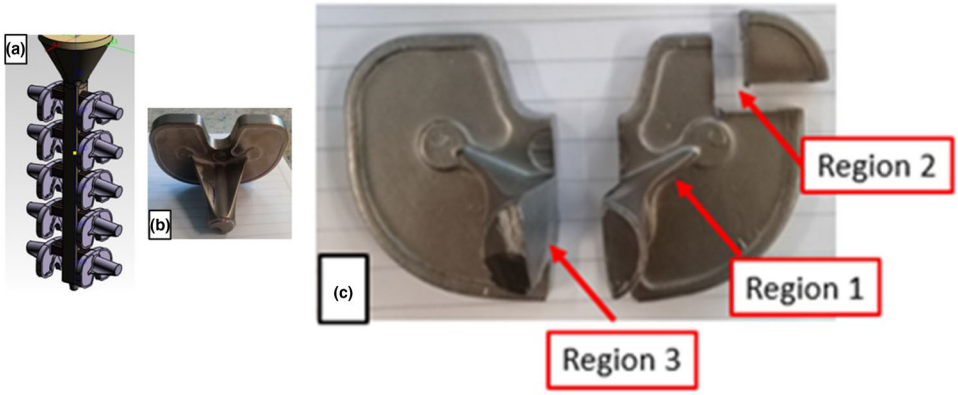

Figure 1. (a) Casting tree, (b) Tibial component and (c) Region 1 (tibial baseplate), Region 2 (Stem reinforcement), Region 3 (Stem).

Table 1. Chemical Composition of the As-cast Co-28Cr-6Mo Alloy (wt%)

Material	Co	Cr	Mo	C	Si	Mn	Ni	Fe
CoCrMo	62.17	29.14	6.35	0.21	0.80	0.57	0.31	0.13
ASTM F75	Bal.	27 -30	5- 7	<0.35	<1.00	<1.00	<0.50	<0.75

into the crucible to remove the oxygen from the melt. After mold filling, a hot topping was added to the top of sprue, and the mold was left open to the atmosphere after the casting.

The investment mold consisted of a colloidal and fused silica base double dip slurry coat, followed by 2 layers of zircon refractory coating and 4 layers of aluminum silicates refractory to give a mold wall thickness of 7 mm. Before pouring, the mold was autoclaved to remove the pattern in a temperature of 195 °C and afterward fired at around 1100 °C. The pouring and mold temperatures employed were 1580 °C and 1050 °C, respectively, and 10 tibial components were simultaneously cast in the casting tree.

Figure 1 shows the casting tree including the tibial components and the three different regions selected for the analysis of the material. It is important to mention that the tibial component, as shown in Figure 1b, was selected randomly from the casting tree (Figure 1a) after knockout.

Three regions were selected to be analyzed, as shown in Figure 1c, based on the differences in wall thickness of the tibial component. The wall thickness of regions 1, 2 and 3 were 1.7 mm, 8 mm and 15.5 mm, respectively. Regions 1, 2 and 3 provided the samples 1, 2 and 3, respectively. The main reason for selecting these regions was to further evaluate the effect of cooling rate on the microstructure and hardness. It should be mentioned that no thermocouple was set up in the mold to measure heat flow during the solidification due to the difficulties to place this device into the mold inside of an industrial foundry plant.

After casting, the samples were then extracted from the selected regions and prepared for the microstructural studies according to ASTM E3. In this case, the samples were mechanically polished with alumina slurry down to 0.3 μm to reach a mirror-like surface effect. At first, the microstructure was evaluated without being etched to determine metallurgical defects such as porosity, inclusions or cracks. After, the samples were etched by immersion during 15 s in a solution of 5 mL HNO_3 + 15 mL HCl to reveal the distribution of phases.

The bulk chemical analysis was performed using optical emission spectroscopy (OES) with the equipment Metal Lab 7580 J. The specimen was analyzed in two spots, and the final chemical composition was determined by calculating the mean values for each element.

The microstructure features were evaluated by optical and scanning electron microscopy (OM and SEM) coupled with energy dispersive spectroscopy (EDS). OM images were obtained using a visible-light microscopy model Olympus BX60M, while SEM images were acquired using a Hitachi-TM1000 scanning electron microscope operating at 15 kV. To estimate the secondary dendrite arm spacing (SDAS) of each specimen, two OM images were chosen, for each image, five different fields were taken into consideration using the software ImageJ®. The same approach was used to determine the size and fraction of carbides.

To identify the phases and estimate their volume fractions, X-ray diffraction (XRD) analysis was conducted. The XRD patterns were obtained by using Cu Kα radiation operating

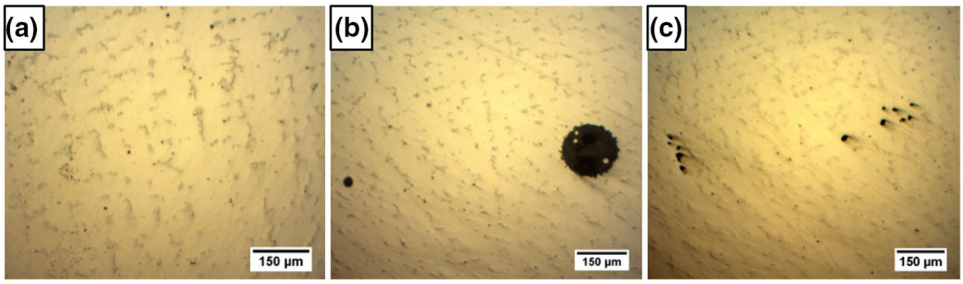

Figure 2. Optical microscopy images of the as-cast Co-28Cr-6Mo alloy taken from the regions of implant: region 1 (a), region 2 (b) and region 3 (c), without being etched.

at 45 kV and 40 mA with a X'Pert Panalytical diffractometer equipped with a graphite monochromator and 2θ angle range from 20 to 90°. The peaks were identified by comparing the experimental data with the database for pure cobalt from ICSD (#52934) and ICSD (#53806).

Vickers hardness was measured using Buehler equipment with a load of 500 gf applied for 10 s. To ensure the accuracy of the results, all the samples were measured five times, and the average value of the measured data was used to indicate the hardness of each sample. Afterward, Vickers hardness was converted to Rockwell C hardness to make a comparison with the ASTM F75 Standard.

Due to the main difficult to set thermocouples in the mold to assess the cooling rates during the solidification of metal in an industrial environment plant, casting numerical simulation was performed to assess the metal flow during filling, and to determine the cooling rates and thermal gradients for each region analyzed in this study during solidification. The casting simulation software used was the Magmasoft version 5.4.1 whose calculation is based on finite volume methods. The finite volume method is an efficient approach to solve differential equations related to heat and mass flow. The cooling rates were determined in the solidification range of the Co-28Cr-6Mo alloy. The input data were the same as the casting parameters utilized in the investment casting process as mentioned previously. The main input data required by the simulation are the following: initial pouring temperature, initial mold temperature, heat transfer coefficients (mold/metal interface), alloy composition and boundary conditions.

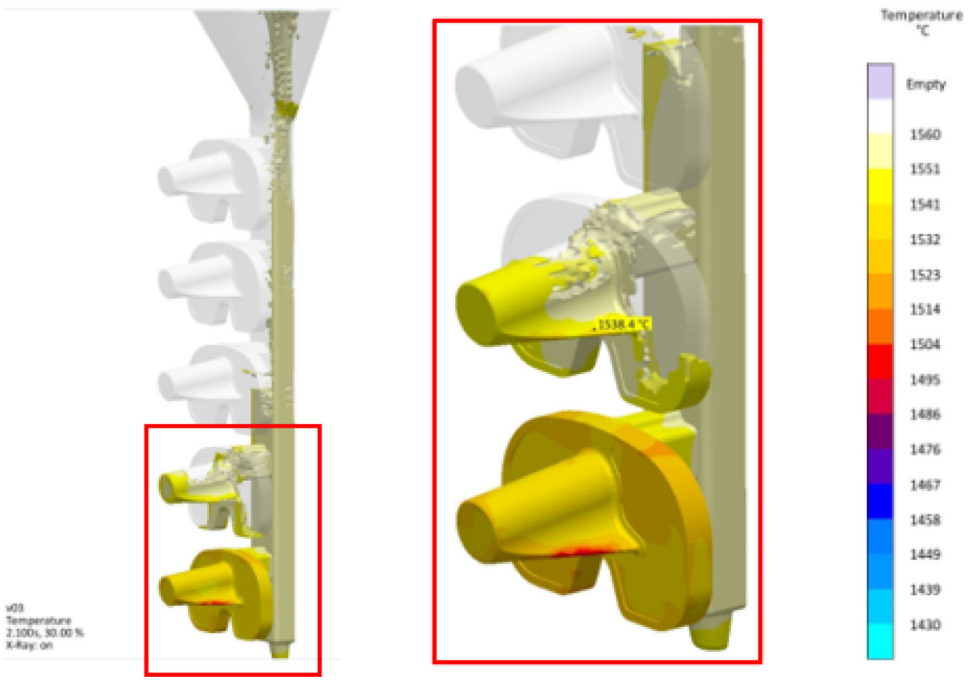

Figure 3. Temperature profile during the filling of the mold cavity as determined by casting simulation in the tibial implant.

Results and Discussions

Chemical Composition

As shown in Table 1, the chemical composition of the as-cast Co-28Cr-6Mo alloy is in good agreement with the ASTM F75 standard. The main alloying elements are Cr, Mo and C. The Cr content is a little superior from the nominal composition (over 1% wt) but it is still in the desired range, whereas the Mo content is close to the nominal composition. A higher concentration of Cr is responsible for stabilizing ε- phase at higher temperatures. [5]It should be mentioned that the carbon concentration must be controlled below 0.35 wt% to avoid an excess of lamellar carbides precipitation at grain boundaries. [8]The Ni content is moderate (0.31 wt%) compared to the maximum standard (0.5 wt%). Even though the ductility can be improved by adding Ni in the alloy, a higher amount of Ni should be avoided once Ni is currently known to be a risk factor for metallic allergy in the human body[16].

Microstructural Analysis

Figures 2a–c show the optical micrographs of the as-cast Co-28Cr-6Mo alloy from regions 1, 2 and 3 of the tibial component (as illustrated in Figure 1), respectively. These images were obtained without being etched to allow the observation of metallurgical defects such as porosity and inclusions. In fact, the presence of porosity and inclusions (indicated as black spots in the images) was observed for the samples taken from regions 2 and 3 of tibial implant as shown in Figure 2b, c, respectively. The gas porosity with a round shape observed in the region 2 has a diameter around 16 µm whereas the inclusions have mean size of 55 µm. In order to distinguish porosity than inclusions, EDS analysis was employed as shown ahead in this study. Fleming et al.[17] also reported shrinkage porosity and micro gas porosity for Co-Cr-Mo alloys, but not metallurgical defects with larger dimensions. The defects observed in this study have larger dimensions than those observed in samples produced in laboratory-scale whose experimental conditions can be better controlled. The area fraction of defects for regions 2 and 3 are 1.5% and 0.5%, respectively. Even considering the fact that the defects observed here were larger than those reported by Giacchi et al.[8], these defects occur isolated and with low area fraction, which is acceptable according to the investment casting standard for Co-Cr-Mo alloys, *ISO 5832-4:2017*. If the area fraction of defects in the tibia baseplate (region 2) is superior to the specification of investment casting standard, mechanical fractures as those reported in literature[13, 15] might occur. The microstructure observed in the region 1 did not reveal the presence of any metallurgical defect.

Casting numerical simulation permitted to assess the molten metal behavior during the filling of the mold cavity. Figure 3 shows the temperature profile determined by casting numerical simulation in the whole volume of tibial implant. The temperature scale showed in Figure 3 contains the maximum and minimum temperatures, which are the pouring and the *liquidus* temperatures, respectively. As we can observe, there was no clear evidence of solidification during the filling because the molten metal temperature was always far above the liquidus temperature. However, the metal flow showed to be turbulent in the first stages of the mold filling, especially in the regions 2 and 3 of the tibial component. The turbulent flow of the liquid metal in the mold cavity favors air entrapment and metal oxidation. Therefore, the regions 2 and 3 are more susceptible to metallurgical defects such as porosity and oxides, as we could see in Figure 2b, c. The region 1 of the tibial component did not reveal any defects because of the laminar behavior of the metal flow in this region.

The presence of oxide inclusions and porosities are detrimental to the mechanical performance of the cast parts because they can act as stress raisers. The main mechanical properties affected by the presence of inclusions are ductility and fatigue strength of the cast component[4].

Figure 4 shows the optical micrographs from the regions 1 to 3, but in this case, the samples were chemically etched to reveal more details of the microstructure, in particular, the dendritic solidification of the as-cast Co-28Cr-6Mo alloy as we can see in these images. Figure 5 is similar to Figure 4, but the micrographs were taken with higher magnification to show in more details the coarse carbides precipitated at interdendritic regions and grain boundaries (which refers to the dark phases in the matrix). As can be noticed in the

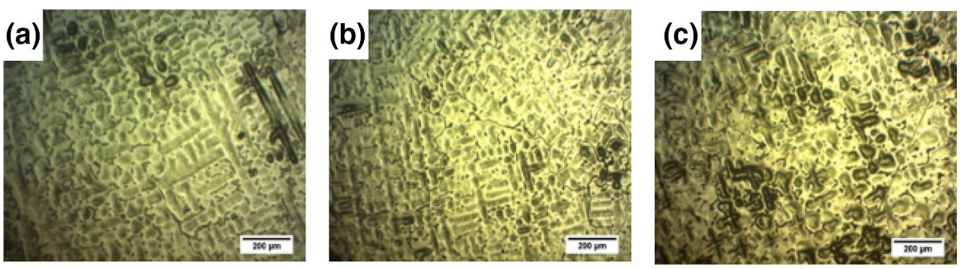

Figure 4. Optical microscopy images of the as-cast Co-28Cr-6Mo alloy taken from the regions of implant: region 1 (a), region 2 (b) and region 3 (c), chemically etched.

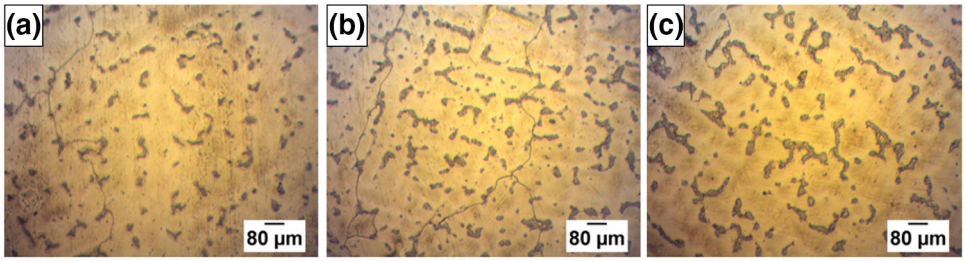

Figure 5. Optical microscopy images of the as-cast Co-28Cr-6Mo alloy taken from the regions of implant: region 1 (a), region 2 (b) and region 3 (c), chemically etched and with higher magnification.

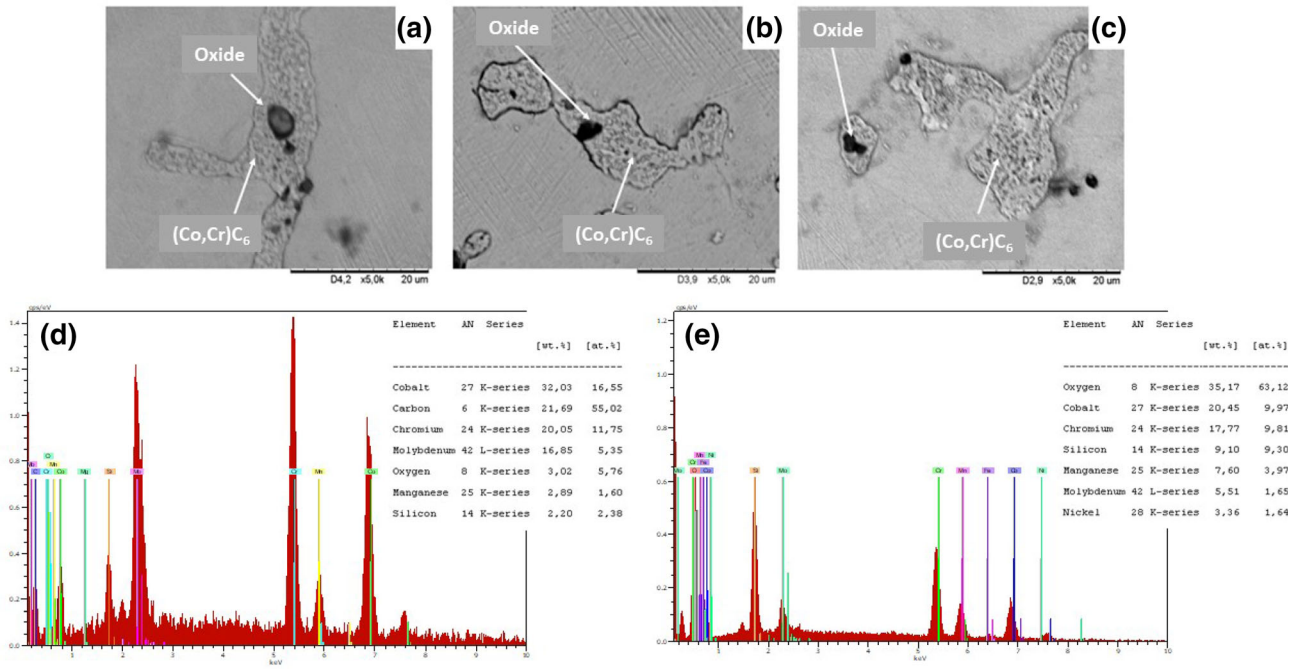

Figure 6. SEM images of the samples taken from: (a) region 1; (b) region 2 and (c) region 3; (d) and (e) EDS spectra taken from the carbide and oxide regions.

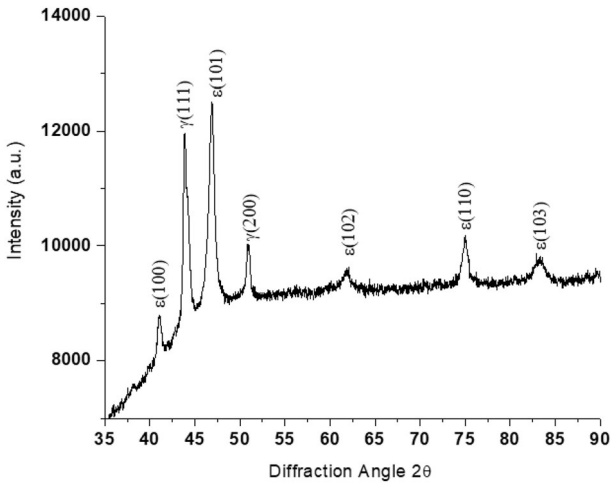

Figure 7. X-ray diffraction pattern of the as-cast Co-28Cr-6Mo alloy.

micrographs of Figure 5, the carbides morphology is characterized as a blocky type nature. These results are consistent with those reported by Giacchi et al.[8] and Kaiser et al.[3] during the analysis of the microstructure of ASTM F75 alloys. The presence of coarse carbides precipitated at interdendritic regions can contribute to reduce the ductility and the corrosion resistance of the alloy in physiological media. [6]So, these results are also in agreement with the references. [8, 18]In many cases, solution annealing heat treatment is often employed on the as-cast parts to promote the carbides dissolution in the matrix.

Figure 5 also shows that the size of carbides and its morphology did not vary significantly from the samples taken from the region 1 to region 2. However, the sample taken from region 3 presented coarser carbides.

Figure 6 shows the SEM images taken from the samples obtained from regions 1, 2 and 3, respectively. EDS spectra

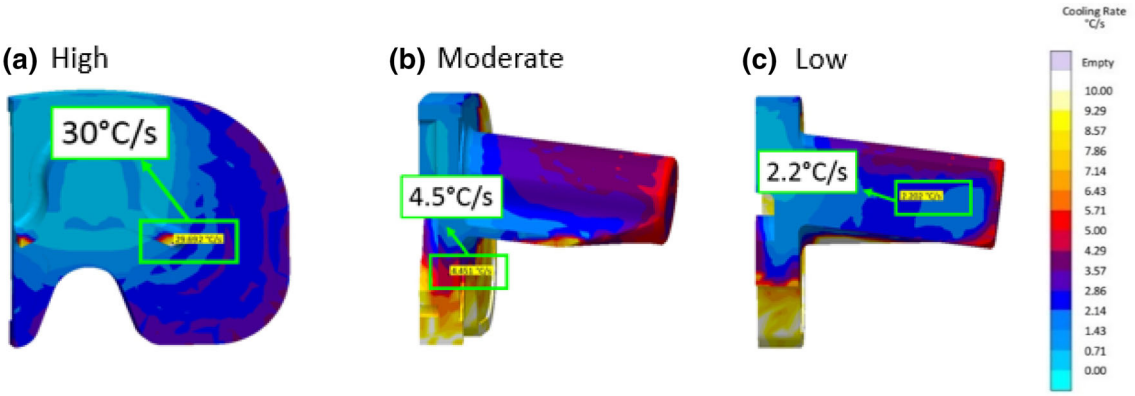

Figure 8. The cooling rates of the samples taken from region 1 (a), region 2 (b) and region 3 (c), as determined by casting numerical simulation. Software clipping tool was used to show the regions in more details.

containing the amount of elements (wt% and at.%) obtained in selected regions from the sample taken from the region 1 is also included in Figure 6. The results confirmed the presence of carbides with chemical composition (rich in: Co, Cr) C_6 precipitated in the grain boundaries and interdendritic regions as indicated by the EDS spectrum shown in Figure 6d. In addition, oxide inclusions rich in O, Co, Cr and Si elements, as detected by EDS spectrum shown in Figure 6e, are also present mainly on the carbides, which suggests that these oxides were dragged onto the carbides during solidification of alloy. [8]These oxides, which are smaller than those observed in Figure 2c, can be classified as endogenous non-metallic inclusions, and they can be controlled by the amount of oxygen dissolved in the molten metal. The investment casting process of the tibial component was carried out in an air atmosphere, which allowed the reaction of the liquid metal with oxygen. Therefore, even though metallic Si was used to remove the oxygen from the liquid metal in the crucible, it was not enough to avoid the presence of large and tiny oxides in the implant. It is well known that the presence of inclusions has a negative effect on fatigue behavior as well as on the corrosion resistance of the alloy[19].

Figure 7 shows the XRD pattern of the as-cast Co-28Cr-6Mo alloy. The XRD showed that the alloy consists of two phases: γ-phase and ε-phase whose crystal structures are face centered cubic (FCC) and hexagonal close-packed (HCP), respectively. These results are in good agreement with the findings of Kajima et al.[1]. The XRD analysis did not reveal the presence of any peaks related to other phases such as carbides and/or σ-phase, even considering the fact that carbides were observed by optical and scanning electron microscopy images (Figures 3, 4 and 6) with an average area fraction between 9 and 11%. This means that the volume fraction of carbides was not superior to 5%, which is the detection limit of the XRD equipment. Sigma phase was reported by Rosenthal et al.[7], but not in the present study, which means that, minor variations in the alloy composition and casting parameters might explain the microstructural differences found in previous studies.

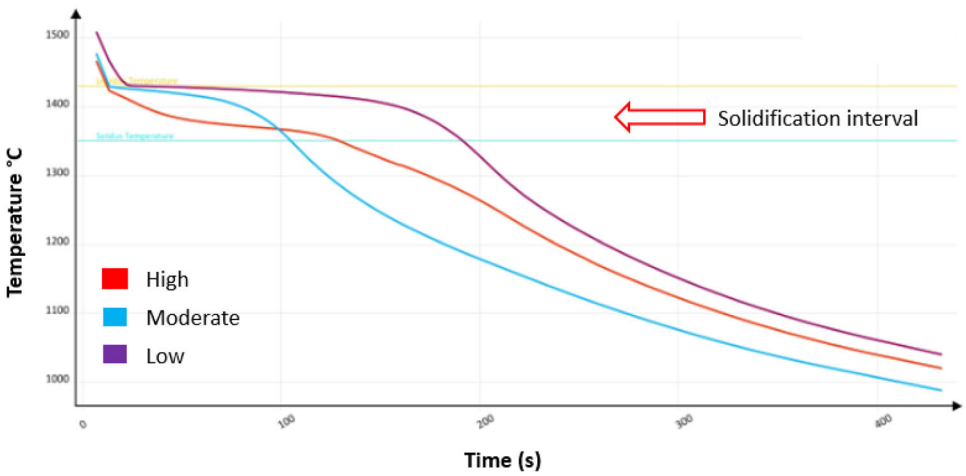

Figure 9. The cooling curves of the region 1 (red), region 2 (blue) and region 3 (purple) as determined by casting simulation.

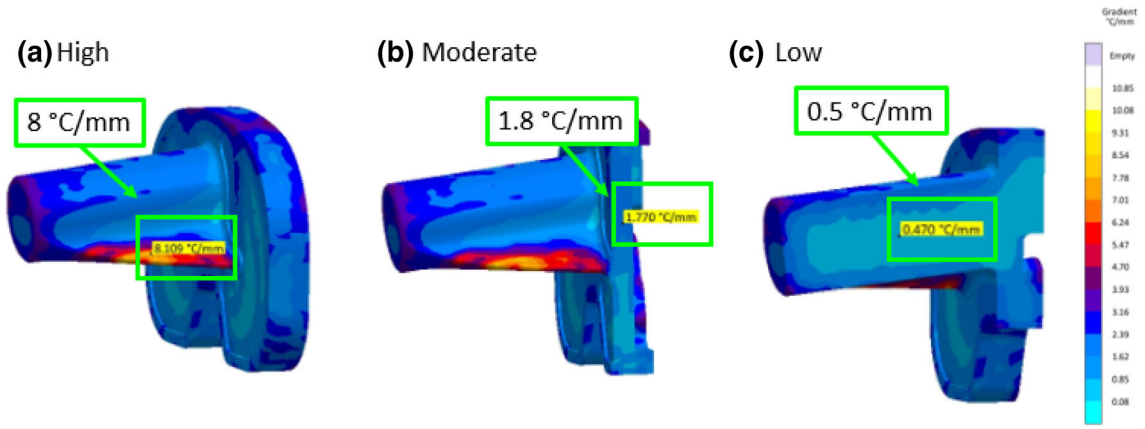

Figure 10. Thermal gradients of samples taken from region 1 (a), region 2 (b), and region 3 (c), as determined by casting simulation.

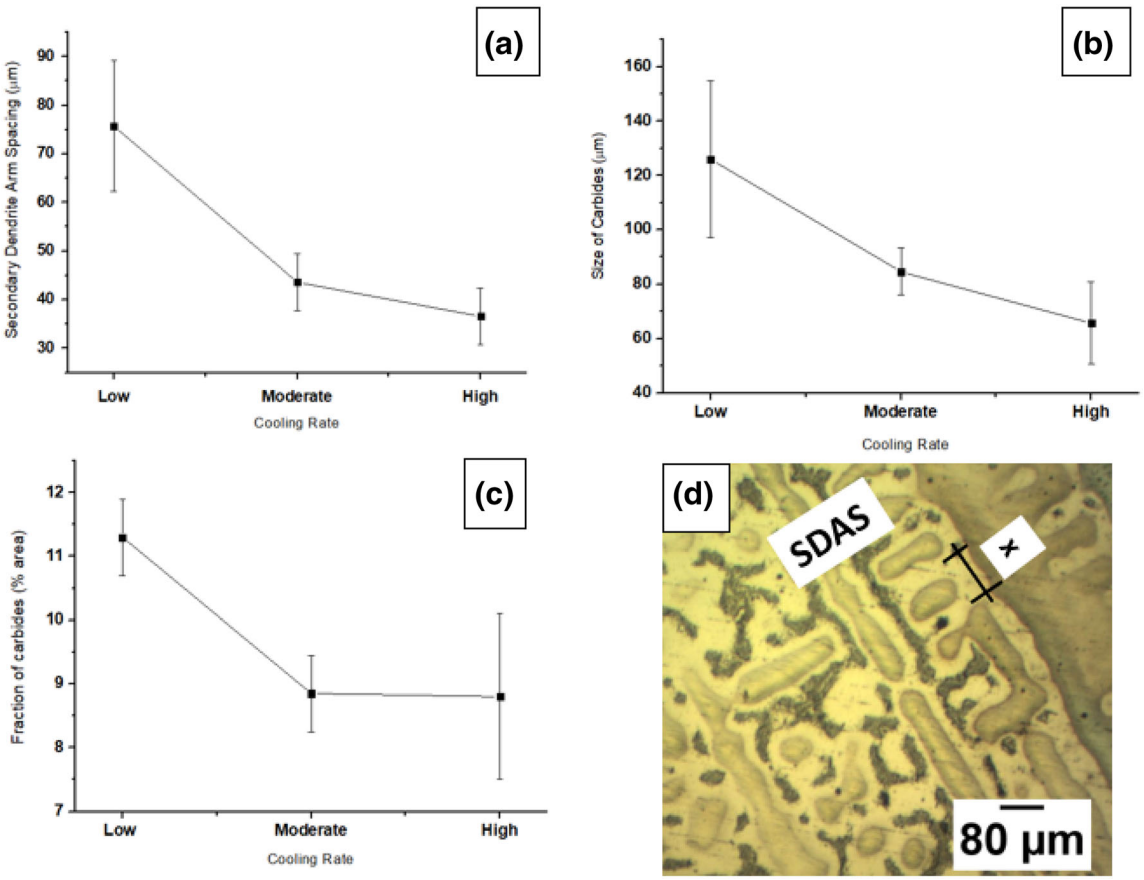

Figure 11. The effect of cooling rate on: (a) the secondary dendrite arm spacing (SDAS), (b) the size of carbides, (c) the area fraction of carbides and (d) SDAS measurement through MO image. Low, Moderate and High cooling rates are directly associated with the samples taken from regions 3, 2 and 1, respectively.

According to the Co-Cr-Mo phase diagram[20], only ε-phase should be present at room temperature. However, due to the slow nature of γ-phase -> ε-phase transformation during freezing, the cooling rate employed by the investment casting processing did not allow the transformation to complete entirely, and as a result, γ-phase is retained at room temperature as a metastable phase.

The volume fraction of both phases can be calculated from the intensities of their XRD peaks using the equation developed by Sage and Guillaud. [21]According to this equation, the results showed that the volume fraction of γ-phase and ε-phase are 59% and 41%, respectively. Therefore, most of the matrix is composed of the metastable γ-phase, which contributes for an increase in ductility of the

alloy since the FCC crystal structure has more slip systems available for plastic deformation in comparison to the HCP crystal structure related to ε-phase.

Casting Numerical Simulation: Cooling Rate and Thermal Gradient

The cooling rates of selected regions 1, 2 and 3 of the tibial implant were determined by casting numerical simulation as can be shown in Figure 8. In this simulation, we applied as input data the same solidification parameters used in the investment casting process, and the cooling rate and thermal gradient were determined within the solidification range of the alloy. The analysis of Figure 8 showed that the region 1 has the highest cooling rate (30°C/s) followed by region 2 (4.5 °C/s) and region 3 (2.2°C/s). Here, it is very important to mention that the different cooling rates are directly associated with the differences on wall thickness among the regions 1, 2 and 3 taken from the tibial implant. Ramírez-Vidaurri et al.[9] also reported the wall thickness influence in the cooling rate by using thermocouples into the mold. The cooling curves were determined with cylinders of different diameters such as 12, 16 and 24 mm, and the average cooling rates were 100, 60 and 20 °C/min, respectively.

The cooling curves of the samples extracted from regions 1, 2 and 3 are exhibited in Figure 9. Within the solidification interval, the red curve is the high cooling rate, the blue curve is the moderate cooling rate, and the purple curve is the low cooling rate, representing the regions 1, 2 and 3, respectively. Figure 10 also shows the temperature gradients (GL) for the liquid ahead to the solid/liquid interface: 8 °C/mm (high), 1.8 °C/mm (moderate) and 0.5 °C/mm (low), which refers to the regions 1, 2 and 3, respectively. As can be observed, there is an interesting relation between cooling rate and thermal gradient. The

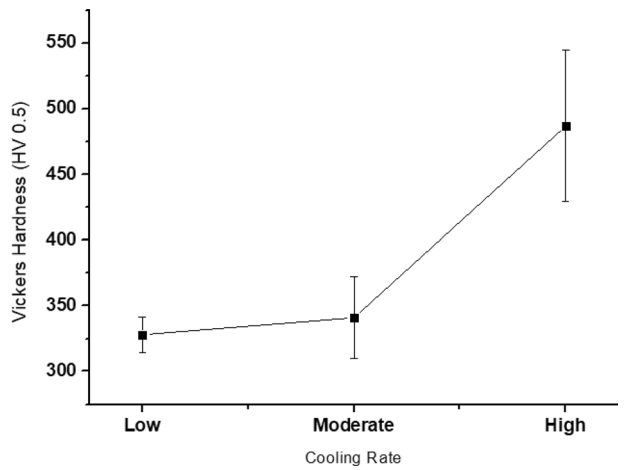

Figure 12. The effect of cooling rate on the hardness of the samples. Low (Region 3), Moderate (Region 2) and High (Region 1).

Table 2. Mean Vickers and Rockwell C hardness of the samples taken from the regions 1, 2 and 3

Samples	Vickers hardness (HV)	Rockwell C hardness (HRC)
1	487	48
2	341	36
3	328	33

higher is the cooling rate, the higher is the thermal gradient, which is in agreement with the simulation data showed in Figure 8 and 10.

Figure 11a shows the cooling rate effect on the secondary dendrite arm spacing (SDAS). It can be seen that the secondary dendrite arm spacing decreases as the cooling rate increases, which is consistent with the results reported by Kaiser et al.[3] At low cooling rates, the mean SDAS value is around 76 µm and drops down to 37 µm at high cooling rates. Figure 11b shows the effect of cooling rate on the size of carbides. As can be observed, the mean size of carbides in the regions 1, 2 and 3 are 65 µm, 84 µm and 126 µm, respectively.

Figure 11c exhibits the effect of cooling rate on the area fraction of carbides. The results show that the average area fraction of carbides is 9, 9 and 11% for the regions 1, 2 and 3, respectively. Therefore, when the cooling rate is high the refinement of the microstructure is favorable, as seen in the optical micrographs images shown in Figure 4 as well as the reduction of the carbides, which can be also observed in Figure 5. These results are consistent with the findings of Kaiser et al.[3] and Toosi et al. [22]On the other hand, the cooling rate did not show a significant effect on the fraction of carbides, which is also in good agreement with the results reported by Ramírez et al. [9]Once the carbides formation is a diffusional process, when the cooling rate is high, the diffusion of C and Cr into the interdendritic and grain boundary regions is suppressed. Besides, the casting parameters such as cooling rate and thermal gradient play a key role in the final microstructure of the alloys. High cooling rates increase the constitutional supercooling in the liquid ahead to the solidification front, which contributes to a dendritic growth during freezing. In addition, the interface solid/liquid moves faster as the cooling rate increases and also favors dendritic solidification. Secondary dendrite refinement occurs at higher cooling rates because the lateral diffusion of the rejected solute is fairly reduced, and, therefore, smaller dendrite arm spacings are necessary to avoid supercooling. [15, 23]Regarding thermal gradient, even though the region 1 presented the highest thermal gradient (8 °C/mm) among the regions selected, it was not sufficient to avoid supercooling and promote planar or cellular growth.

Vickers Hardness

Figure 12 exhibits the effect of cooling rate on the hardness of the samples taken from the regions 1, 2 and 3. The results show that there is a strong relationship between the cooling rate and the hardness, which is consistent with the findings reported in literature. [3, 22]As the cooling rate increases, the hardness of the samples increases as well due to the secondary dendrite arm spacing refinement, as mentioned in Figure 11a. This relation between cooling rate and hardness is also observed in other alloys such as cast steels and aluminum alloys. [4]The average hardness values of the samples extracted from the regions 1, 2 and 3 are 487 HV, 341 HV and 328 HV, respectively, and are reported in Table 2. The samples taken from regions 1 and 2 exhibited hardness higher than those required by ASTM F75 Standard (25–35 HRC).

For Co-based alloys, ε-phase contributes to increase the hardness of alloy. As the XRD analysis showed, a volume fraction of around 41% of ε-phase was found in the as-cast alloy. Therefore, it is expected that all the samples exhibit a similar volume fraction of this phase because the γ-phase -> ε-phase transformation under cooling takes place at 970 °C, and at this temperature, there is no significant differences in the cooling rates for regions 1, 2 and 3 (Figure 8) that could change the volume fraction of each phase significantly. So, the dendrite refinement must be the major reason for the high value of hardness in the sample taken from region 1.

Parts of the implant with high hardness values can lead to low ductility, which can cause brittle failure when submitted to cyclic loads. [3]Therefore, the tibial component in the as-cast condition is more prone to have brittle failure in the regions 1 and 2 as already reported by the studies with focus on the investigation of premature failures on knee implants[13, 15]. Hence, the use of a knee implant in the as-cast condition is not recommended, and heat treatments are usually employed for these alloys[2], even though thermal process is not mandatory according to the ASTM F75 Standard.

Conclusions

In this study, we investigated the microstructural features of three different regions of a tibial component used as knee implant with composition of Co-28Cr-6Mo alloy produced by investment casting under industrial environment. A special attention was paid in the effects of cooling rate experienced by these regions on the microstructure and hardness of the alloy. The following conclusions could be drawn from this investigation:

(1) The microstructure of the as-cast Co-28Cr-6Mo consisted of two phases: γ-phase and ε-phase with volume fraction as determined by XRD of around 59% and 41%, respectively. The presence of carbides with composition of $(Co,Cr)C_6$ was also found precipitated in the grain boundary and interdendritic regions;

(2) Porosity and oxides were observed in the implant mainly in regions that experienced turbulent flow during filling of the molten metal. In addition, tiny oxides were also observed on the carbides in the grain boundaries;

(3) The effect of cooling rate on the fraction of carbides was not significant. However, higher cooling rates promoted the formation of smaller carbides;

(4) The region of the implant that experienced the highest cooling rate exhibited the highest hardness due to the grain refinement;

Finally, this study showed that there were significant microstructural differences in the as-cast tibial component used as a knee implant produced by investment casting mainly due to the geometry changes, which led to distinct cooling rates during the solidification process resulting in the presence of metallurgical defects in different regions of implant and also differences on hardness. As a result, the great variation in hardness exhibited by the implant might be a wake-up call once brittle failure is favored by high hardness values. Therefore, the use of a knee implant produced by investment casting with Co-28Cr-6Mo alloy is not recommended in the as-cast condition, and heat treatment should be carried out to minimize microstructural and hardness differences as observed in this study. Mechanical fractures in tibial components are rare but if the defects pointed out by this study take place in larger fractions, tibia baseplate fracture might occur catastrophically.

Acknowledgements

The authors gratefully acknowledge Fundimazza Investment Casting Foundry for the financial support of this study.

REFERENCES

1. K. Yuka et al., Effect of heat treatment temperature on microstructure and mechanical properties of Co-Cr-Mo alloys fabricated by selective laser melting. Mater. Sci. Eng. A **726**, 21–31 (2018). https://doi.org/10.1016/j.msea.2018.04.048
2. C. Valero-Vidal et al., Influence of carbides and microstructure of CoCrMo alloys on their metallic dissolution resistance. Mater. Sci. Eng. C **33**, 4667–4676 (2013). https://doi.org/10.1016/j.msec.2013.07.041
3. R. Kaiser et al., The influence of cooling conditions on grain size, secondary phase precipitates and

mechanical properties of biomedical alloy specimens produced by investment casting. J. Mech. Behav. Biomed. Mater. **24**, 53–63 (2013). https://doi.org/10.1016/j.jmbbm.2013.04.013
4. ASM International. Casting. In: ASM Handbook. 9th. Ed. ASM International, V.15, (2008)
5. J.B. Park et al., Microstructure of As-Cast Co-Cr-Mo alloy prepared by investment casting. J. Korean Phys. Soc. **72**, 947–951 (2018)
6. G. Herranz et al., Mechanical performance, corrosion and tribological evaluation of a Co-Cr-Mo alloy processed by MIM for biomedical applications. J. Mech. Behav. Biomed. Mater. **105**, 1–11 (2020). https://doi.org/10.1016/j.jmbbm.2020.103706
7. R. Rosenthal et al., Phase characterization in As-Cast F75 Co-Cr-Mo Alloy. J. Mater. Sci. **45**, 4021–4028 (2010)
8. J.V. Giacchi et al., Microstructural characterization of As-cast biocompatible Co-Cr-Mo alloys. Mater. Charact. **62**, 53–61 (2011). https://doi.org/10.1016/j.matchar.2010.10.011
9. L.E. Ramírez-Vidaurri et al., Cooling rate and carbon content effect on the fraction of secondary phases precipitate in as cast microstructure of ASTM F75 alloy. J. Mater. Process. Technol. **209**, 1681–1687 (2009). https://doi.org/10.1016/j.jmatprotec.2008.04.039
10. M. Caudillo et al., On carbide dissolution in an as-cast ASTM F-75 alloy. J. Biomed. Mater. Res. **59**, 378–385 (2002). https://doi.org/10.1002/jbm.10001
11. Y. Bedolla-Gil et al. Influence of heat treatments on mechanical properties of a biocompatility alloy ASTM F75. Revista Mexicana de Física [en linea]. 2009, 55(1), 1-5[fecha de Consulta 13 de Diciembre de 2021]. ISSN: 0035-001X. Disponible en: https://www.redalyc.org/articulo.oa?id=57030347001
12. M.A. Hernandez-Rodriguez et al., Tribological performance of CoCrMo alloys with boron additions in As-Cast and heat-treated conditions. Metals **11**, 355 (2021). https://doi.org/10.3390/met11020355
13. S. Rytter et al., Implant fracture of the regenerex modular metal tibial component: a report of three cases. Knee **26**, 1143–1151 (2019). https://doi.org/10.1016/j.knee.2019.06.009
14. J. Singh et al., Rates of total joint replacement in the united states: future projections to 2020–2040 using the national inpatient sample. J. Reumathol. **49**, 1134–1140 (2019). https://doi.org/10.3899/jrheum.170990
15. I.M. da Palma et al., Fracture of the tibial component in total knee arthroplasty: report on two cases. Revista Brasileira de Ortopedia **46**, 325–328 (2011). https://doi.org/10.1016/S2255-4971(15)30205-6
16. K. Yoda et al., Effects of chromium and nitrogen content on the microstructure and mechanical properties of As-Cast Co-Cr-Mo alloys for dental applications. Acta Biomater. **8**, 2856–2862 (2012). https://doi.org/10.1016/j.actbio.2012.03.024
17. T. Fleming et al., The effect of induction heating power on the microstructural and physical properties of investment cast ASTM F75 CoCrMo alloy. J. Mater. Res. Technol. **8**, 4417–4424 (2019). https://doi.org/10.1016/j.jmrt.2019.07.052
18. E. Almanza-Casas, M.J. Pérez-López, N.A. Rodríguez-Rosales, Effect of heat treatment on the corrosion resistance in a Co–28Cr–6Mo alloy casting for surgical implants. Inter. Metalcas.t **12**, 71–78 (2018). https://doi.org/10.1007/s40962-017-0139-6
19. Bettini, Eleonara. Influence of Carbides and Nitrides on Corrosion Initiation of Advanced Alloys—A Local Probing Study. 2013. 73 f. Doctoral Thesis - School of Chemical Science and Engineering, Royal Institute of Technology, Stockholm, 2013.
20. Antunes, Luiz Henrique Martinez. Caracterização da Liga Co28Cr6Mo Obtida por Manufatura Aditiva e por Microfundição. 2017. 88 f. Dissertação (Mestrado) - Curso de Engenharia Mecânica, Universidade Estadual de Campinas, Campinas, 2017
21. M. Sage, C. Guillaud, Méthode d′analyse quantitative des variétés allotropiques du cobalt pre les Rayons X. Rev. Metall **49**, 139–145 (1950). https://doi.org/10.1051/metal/195047020139
22. Toosi, Hamid Reza Erfanian Nazif. The Effect of Rapid Solidification and Heat Treatment on Microstructure and Electrochemical of Advanced Biomaterial Co-Cr-Mo Alloy. 2019. 142 f. Doctoral Thesis - Philosophy in Engineering, University of Wisconsin-Milwaukee, Milwaukee, 2019.
23. D.A. Porter, *Phase Transformations in Metals and Alloys*, 3rd edn. (Crc Press, New York, 2008), p. 491